Z. Phys. C – Particles and Fields 50, 293–304 (1991)

Zeitschrift für Physik C Particles and Fields

Deep inelastic Compton scattering at the *ep* collider HERA

A.C. Bawa[1,a], Maria Krawczyk[1,b], W.J. Stirling[2]

[1] Deutsches Elektronen-Synchrotron DESY, W-2000 Hamburg 52, Federal Republic of Germany
[2] Departments of Physics and Mathematical Sciences, Durham University Durham, UK

Received 19 October 1990

Abstract. Deep inelastic Compton scattering at HERA is investigated with the intention of determining the usefulness of this process in pinning down the photon and proton structure functions. We examine the contributions of the various $\alpha\alpha_s$ and α_s^2 subprocesses that arise from the nonelementary structure of the photon at $S_{\gamma p} = 30000\,\mathrm{GeV}^2$. An assessment is made of the sensitivity of this process to the various parton and photon structure functions presently available. In particular we study the possibility of directly measuring the gluon content of the proton and the photon as well as the quark fragmentation into a photon with this process. The *ep* laboratory frame helps to separate out the different contributions and in particular may allow a quantitative study of the box diagram term.

1 Introduction

The primary programme of the soon-to-be running *ep* collider HERA will be to study with accuracy the structure of the proton in regions that are not accessible at present experiments. The proton will be probed at HERA with highly virtual photons up to $Q^2 \sim 10^5\,\mathrm{GeV}^2$ and for x down to 5×10^{-5} [1]. Another avenue that may be considered at HERA is that of the photoproduction processes in which the protons interact with nearly real photons ($Q^2 \simeq 0$). The average centre-of-mass energy for these events is predicted to be $\sqrt{S_{\gamma p}} \sim$ 170–200 GeV [2].

In this study we consider the simplest inclusive photoproduction process: deep inelastic Compton (DIC) scattering in which photons with large transverse momentum, p_T^γ, are produced. Some aspects of this process at HERA have already been discussed in the literature [3,4]. In earlier studies [5,6] we investigated the sensitivity of this process to the proton structure function and the effect of the structure of the photon on the cross sections.

The DIC process occurs at lowest order in α_s, that is α_s^0, via the elementary Compton scattering of photons on quarks: $\gamma + q \to \gamma + q$. The complete next-to-leading order calculation has been performed [7–9] and some approximated all orders results exist in the literature [10,11]. The structure of the next-to-leading order corrections are considerably simpler than in the case of the hadronic counterpart of this process because of the point-like couplings of the photons to quarks in the initial and final channels. This feature makes the process an important test of perturbative QCD [12]. The $O(\alpha_s)$ contribution to the differential cross section $d\sigma/dp_T^\gamma$ has been checked against NA14 data [13] and found to be well under control [5,8]. These data were accumulated with $\sqrt{S_{\gamma N}} \simeq 13\,\mathrm{GeV}$ and $p_T^\gamma < 4\,\mathrm{GeV/c}$.

Since the energy expected for the DIC process at HERA will be much higher, $\sqrt{S_{\gamma p}} \sim 170$–$200\,\mathrm{GeV}$, QCD tests in a much wider range of p_T^γ, up to $\sim 80\,\mathrm{GeV/c}$ can be performed. In the large p_T^γ region $-x_T = 2p_T^\gamma/\sqrt{S_{\gamma p}}$ bigger than 0.3–0.4 – the simple Compton subprocess $\gamma q \to \gamma q$ dominates the cross section. In this case the DIC scattering offers an alternative probe of the quark structure of the proton [5,6,11]; that is, by two electromagnetic probes with a Q^2 scale that is related to be hardness of the process, e.g. $Q^2 = (p_T^\gamma)^2$. This method is of course much more uncertain than the standard DIS experiments but may complement them, particularly in regions of (x, Q^2) which are not accessible in the forthcoming DIS experiments [6].

The differential cross sections at low and moderate p_T^γ are dominated by subprocesses which are due to the partonic interaction of cascades from the proton and the photon. These events are similar to purely hadronic processes and their rates depend not only on the parton densities of the proton but also on the probability of finding partons in the initial photon and/or on the probability that the final state parton will fragment into a photon.. The question that then arises is whether the

[a] Permanent address: University of Durban–Westville, Durban, S. Africa
[b] On leave of absence from Institute of Theoretical Physics, Warsaw University, Warsaw, Poland

DIC process can be utilised to measure the structure of the photon or the fragmentation function involved [3, 4, 6]. The importance of this measurement is related to the fact that, as in the case of hadrons, experimental information is required to determine the structure of the photon. The earlier hope that the QCD structure and fragmentation functions of the photon would be completely calculable [14] is no longer valid [15].

At the present time, the direct determination of the structure function and quark distributions in the photon is being performed in inclusive e^+e^- annihilation via the probing of an almost real photon (the target) by a highly virtual one (the probe); that is, the $\gamma^*\gamma$ process [16]. This is an analogue of the DIS probe of the proton. The determination of the gluon content of the photon and proton requires a new strategy since the electromagnetic probe is insensitive to the gluon. The same applies for the proton where the DIS experiments do not measure the gluons directly and for which the momentum sum rules [17], and hadron–hadron collisions with simple final states, for example $pp \to \gamma X$ [18], are used to determine the gluon distribution. A further method is one in which the gluon content of the proton is obtained from the Altarelli–Parisi evolution equations [19].

For the photon the situation is very similar. However, the sum rule analysis does not apply. Recently, two processes have been proposed to measure the parton (and mainly the gluon) content of the photon in high energy γp collisions at HERA:

$$\gamma p \to J/\psi g \quad [20] \tag{1}$$

$$\gamma p \to j_1 j_2 \quad [21] \tag{2}$$

where j_1 and j_2 are final-state jets. Note that both these reactions can be exploited as mechanisms for probing the gluon structure of the proton as well. Now we can add the deep inelastic Compton scattering [3–6]

$$\gamma p \to \gamma X \tag{3}$$

as a candidate process for the measurement of the parton content, in particular the gluon content, of the photon as well as the proton.

It should be noted that the DIC process may also provide the opportunity to investigate the fragmentation functions of the photon. We are not aware of any measurements of these functions. In principle, these functions may be investigated in e^+e^- annihilation into two jets, at least for $q \to \gamma$. The fragmentation function of the gluon, $D_{\gamma/g}$, describing the decay process $g \to \gamma$, can be directly related to the gluon distribution in the photon; that is, $D_{\gamma/g} = F_{g/\gamma}$ [7]. On the other hand since high energy hadron–hadron collisions are dominated by gluonic interactions, this may provide us in future with the desired information on the fragmentation of the gluon into a photon. We discuss the sensitivity of DIC scattering to the different types of fragmentation functions for $q \to \gamma$ and $g \to \gamma$.

In this paper we examine the main features of the DIC process at the energy expected to be accessible at HERA. The aim is to investigate whether the DIC process can be used for the determination of structure functions of the photon and proton as well as the fragmentation functions $D_{\gamma/q}$ and $D_{\gamma/g}$. Compared to our earlier studies [5, 6], we focus our attention in this paper on the sensitivity of the DIC process cross sections to the different parton parametrizations for the photon and on the topology of the events. In addition we have included the full set of $O(\alpha_s^2)$ subprocesses whereas in [6] we neglected gluon–gluon scattering and the terms which contain $D_{\gamma/g}$. A more detailed investigation based on a Monte Carlo program for HERA is being prepared [22].

We start with the simplifying assumption that at HERA we deal with a beam of real photons with fixed energy, which in accordance with the estimate in [2], we take equal to ~ 9 GeV. The square of the total energy in the centre-of-mass system is $S_{\gamma p} = 30\,000\,\text{GeV}^2$ for the γp collision. In Sect. 2 we provide a review of the photon structure and fragmentation functions used in this study. In Sect. 3 we describe the set of MRS proton structure functions. In Sect. 4 we present the various contributions to the deep inelastic Compton scattering: (a) the $O(\alpha_s)$ corrections to the basic Compton process, (b) the $\alpha_s\alpha$ subprocesses, (c) the α_s^2 subrocesses and (d) the box diagram. Note that the (b) and (c) subprocesses arise from the nonelementary behaviour of the interacting photons and the relevant fragmentation functions. In Sect. 5, cross-section calculations are presented with some analysis of the potential that this process has for studying the structure of the proton and the photon. We perform this calculation in the centre-of-mass frame for the γ-proton collision. We provide a short discussion of the kinematics at HERA and the characteristics of the final states. Finally, in Sect. 6 we draw some conclusions.

2 Parton parametrizations for the photon

The study of the hadronic structure of the photon is becoming increasingly important. The efficient study of two-photon physics at LEP and TRISTAN will depend on the availability of well-constrained photon structure functions. The study of structure functions of the proton at HERA will require a critical handle on the background due to processes in which the photon acts as a hadron. In addition, the discrepancy between the measured cosmic-ray parton showers and the 'standard' calculations is being redressed by including in these calculations the role played by the hadronic nature of photons [23]. After Witten suggested [14] that in the case of infinite momentum transfer the quark and gluon distributions in the photon were exactly calculable, the study of the hadronic structure of photons became a testing arena for perturbative QCD.

2.1 Structure functions

We have used three different functions for the quark distributions in the photon: the parton model (PM) formula [8, 14], the parametrizations of Duke and Owens (DO) [7] and those of Drees and Grassie (DG) [24]. Leading-order analogues of the solutions of the hadronic Altarelli–Parisi equations contain a part which may be calculated [14] in the region of very high Q^2. Unfor-

tunately these 'asymptotic' solutions lead to divergences in F_2^γ as $x \to 0$ and this problem accentuates in higher orders of perturbation theory [15]. The DO set of distributions is a parametrization of the asymptotic part. However, the subasymptotic contributions to the parton distributions are not negligible [24] and so these high Q^2 solutions may be unreliable. The 'parton model' does not make predictions for the gluon distribution in the photon.

An alternative approach is to input quark and gluon distributions from experimental data at some scale Q_0^2. This guarantees a finite F_2^γ at all values of x, Q^2. Drees and Grassie [24] adopt this approach and their input distributions, at $Q_0^2 = 1\,\text{GeV}^2$, are chosen so that their parametrization reproduces existing data. We used this parametrization with the number of quarks set to four and the QCD parameter $\Lambda_{\text{QCD}}^{(4)}$ set equal to 400 MeV. Note that the approach used by DG includes automatically the non-perturbative component of the photon structure function whereas the other two take into account only the perturbative part. A sensitivity to these parametrizations will provide the opportunity to probe this non-perturbative region.

2.2 *Fragmentation functions*

For the fragmentation functions which describe the decays of quarks into final photons we use the (PM) formulae [8, 14] and the DO parametrizations [7]. There is no analogue of the DG parametrization for the fragmentation functions of the photon. The only parametrization that exists for gluons fragmenting into photons is that of DO. As noted above, it is obtained simply by equating $D_{\gamma/g}$ to $F_{g/\gamma}$. In this sense we use for comparison the gluon component of the DG parametrizations as another example of $D_{\gamma/g}$. We can say nothing about the nonperturbative component in the fragmentation function of the photon at the present time.

3 Proton structure functions

In this study we used the MRS set of quark and gluon parametrizations [25, 26] for the proton. They provide a wide variety and include sets that cater for uncertainties that do not originate in poor statistics; for example, the BCDMS-EMC controversy in quark distributions in the nucleons. These parameterizations employ next-to-leading order QCD (in the $\overline{\text{MS}}$ scheme) and the parton densities are presented in (x, Q^2) arrays.

The first set of parametrizations MRS1, 2, 3 [25] were built on the EMC data up to 1987 and these were combined with CDHSW and CCFRR data (including the required renormalisation). The three sets differ in the choice of input gluons and the resulting Λ_{QCD} scales.

MRS1: $xG(x, Q_0^2) \sim (1-x)^5$ and $\Lambda_{\overline{\text{MS}}} = 107\,\text{MeV}$;

MRS2: $xG(x, Q_0^2) \sim (1-x)^4(1+9x)$ and $\Lambda_{\overline{\text{MS}}} = 250\,\text{MeV}$;

MRS3: $xG(x, Q_0^2) \sim 1/\sqrt{x}(1-x)^4(1+9x)$ and $\Lambda_{\overline{\text{MS}}} = 178\,\text{MeV}$.

The reference scale is chosen to be $Q_0^2 = 4\,\text{GeV}^2$, the number of flavours is set to four and the sea is $SU(3)_{\text{flavour}}$ symmetric. The choice of gluons specifies MRS1 as the soft set, MRS2 as the hard set and finally MRS3 as the $1/\sqrt{x}$ set.

A new set of parametrizations was published recently [26]. The MRS1 set was fitted with BCDMS data rather than EMC data. The authors found that this new set fit the Drell–Yan data better than the previous sets. The new sets are modified versions of MRS1, with MRSE′ being based on the EMC parton distributions while MRSB′ is the BCDMS set.

MRSE′: $xG(x, Q_0^2) \sim (1-x)^{4.4}$ and $\Lambda_{\overline{\text{MS}}} = 100\,\text{MeV}$;

MRSB′: $xG(x, Q_0^2) \sim (1-x)^{4.4}$ and $\Lambda_{\overline{\text{MS}}} = 200\,\text{MeV}$;

In this case the bottom quark is included in the analysis.

Finally, the range of applicability is $10^{-4} < x < 1$ and $5\,\text{GeV}^2 < Q^2 < 10^6\,\text{GeV}^2$.

4 The subprocesses and γp kinematics

The process under consideration is DIC scattering at HERA, in which a nearly real photon emitted by an incoming electron, with energy 30 GeV, interacts with an incoming 820 GeV proton, producing a large transverse momentum photon in the final state. We assume a fixed energy for the emitted photons to be 9.15 GeV and this corresponds to $S_{\gamma p} = 30\,000\,\text{GeV}^2$. The lowest-order Born term, shown in Fig. 1, occurs at $O(\alpha^2)$ and is due to photon–quark scattering.

$$\gamma + q \to \gamma + q. \tag{4}$$

The contribution of this subprocess to the cross secction depends on the charge of the quarks to the fourth power. If this contribution is untangled from the rest of the cross section this would confirm the fractional charge of the quarks [27].

The next set of subprocesses, shown in Fig. 2, are at $O(\alpha\alpha_s)$ and originate from the nonelementary behaviour of the incoming photons. The contribution of these processes to the DIC cross section is formally of the same order as the Born term contribution, since the photon structure function is proportional to $\log(Q^2)$ which is $O(1/\alpha_s)$. If we define the generic process to be $a + b \to c + d$, where a represents the photon or its constituent partons, b the proton constituents, and c the final-state observed photon (or its parent parton, which we consider below) then the subprocesses shown in Fig. 2

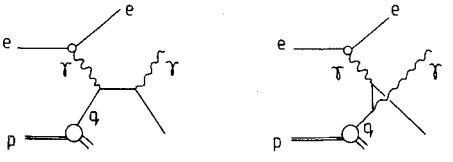

Fig. 1. The Born-level contribution to deep-inelastic Compton scattering: $\gamma + q \to \gamma + q$

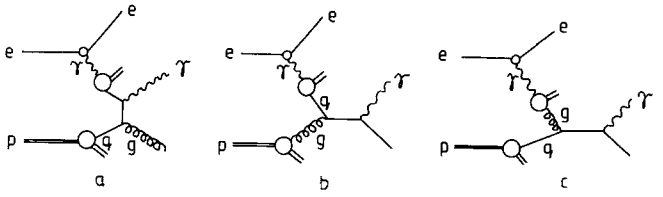

Fig. 2 a–c. The leading-logarithm diagrams due to the photon structure function, at $O(\alpha\alpha_s)$. In **a** and **b** the hard interactions involve quarks from the photon and in **c** a gluon from the photon. The crossed diagrams are not shown

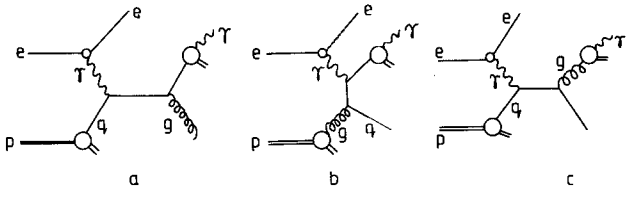

Fig. 3 a–c. The diagrams describing those processes that have an elementary photon in the initial state and a final-state photon that results from a fragmenting quark **a, b** or fragmenting gluon **c**. The crossed diagrams are not shown

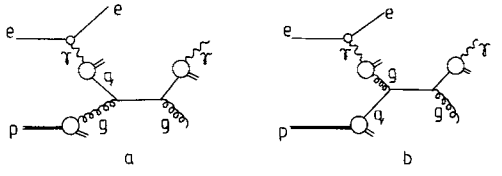

Fig. 4 a, b. Leading-logarithm diagrams which exhibit both hadronic photon behaviour and parton fragmentation in the final-state. In **a** the hard interaction comprises a quark from the photon and a gluon from the proton. In **b**, we have a gluon from the photon interacting with a quark from the proton. The crossed diagrams are not shown

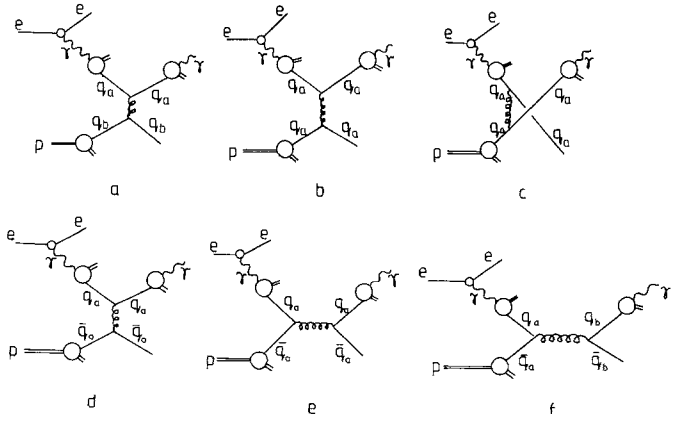

Fig. 5 a–f. Leading-logarithm diagrams with various combinations of quarks and antiquarks in the initial state *and* with the quark fragmentation functions in the final state. The crossed diagrams are not shown

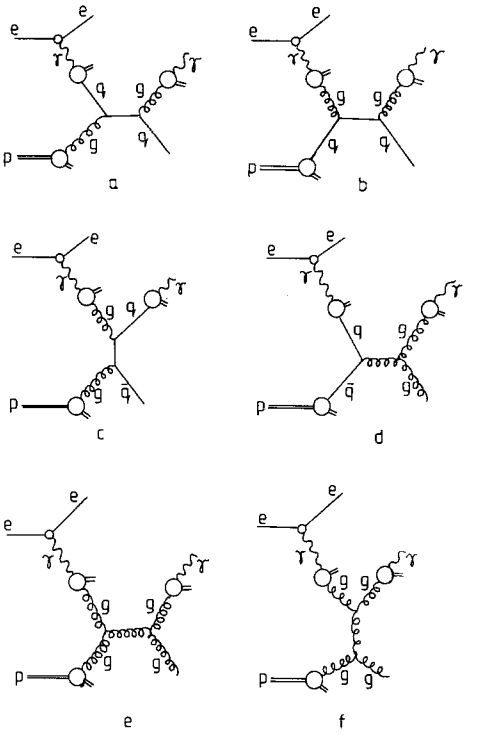

Fig. 6 a–f. Diagrams which have initial-state gluons from the photon, **b, c** and final-state gluons which fragment **a, b, d**. $g+g\to g+g$ diagrams included with the final-state gluon fragmentation **e, f**. The crossed diagrams are not shown

are

$$\begin{aligned}&\bar{q}+q\to\gamma+g\\&q+g\to\gamma+q\\&g+q\to\gamma+q\\&\quad(q\leftrightarrow\bar{q}).\end{aligned}\tag{5}$$

The terms that contain only the fragmentation function of a parton to a photon in the final state are of the same order as the terms above. They are characterised by an elementary photon in the initial state (see Fig. 3),

$$\begin{aligned}&\gamma+q\to q+g\\&\gamma+g\to q+\bar{q}\\&\gamma+q\to g+q.\end{aligned}\tag{6}$$

In these processes (5, 6) we used the matrix-element expressions of Duke and Owens [7].

The other contributions that we take into account are those in which the initial-state photon behaves hadronically and one of the final-state partons fragments into a photon. These are nominally at $O(\alpha_s^2)$ but are again at the order of the Born term if we consider that both the fragmentation and photon structure function terms have factors (α/α_s). The diagrams, shown in Figs. 4–6, are

$$\begin{aligned}&q+g\to q+g\\&g+q\to q+g\\&q_a+q_b\to q_a+q_b\\&q_a+q_a\to q_a+q_a\\&q_a+\bar{q}_a\to q_a+\bar{q}_a\end{aligned}$$

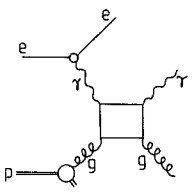

Fig. 7. The box diagram contribution to the Compton process, $\gamma + g \to \gamma + g$. The crossed diagram is not shown

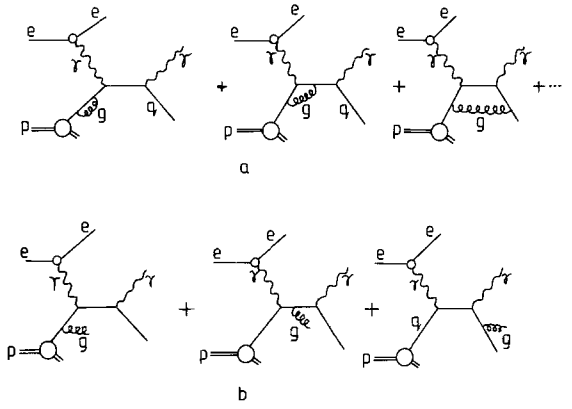

Fig. 8a, b. $O(\alpha\alpha_s)$ virtual diagrams which interfere with the Born diagram to produce $O(\alpha_s)$ corrections, **a**. **b** real $O(\alpha_s)$ corrections to the Born diagram. The crossed diagrams are not shown

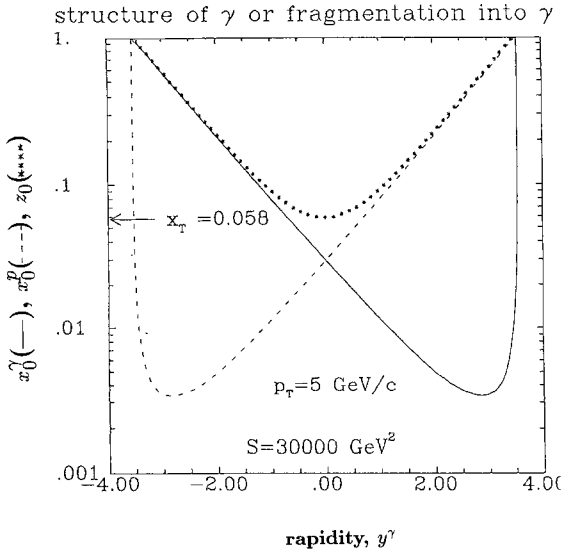

Fig. 9. The kinematics of the DIC process at $S = 30\,000\,\mathrm{GeV}^2$ corresponding to the Born process. x_0^γ and x_0^p are the minimum values for the photon and proton momentum fractions with $p_T^\gamma = 5\,\mathrm{GeV/c}$, as a function of the rapidity of the final-state photon. z_0 is the minimum value of the fragmentation variable for the same kinematic parameters. Then x^γ, x^p and z lie between these minimum values on the curves and 1. (Taken from [6])

$$
\begin{aligned}
&q_a + \bar{q}_a \to q_b + \bar{q}_b \\
&q + g \to g + q \\
&g + q \to g + q \\
&g + g \to q + \bar{q} \\
&q + \bar{q} \to g + g \\
&g + g \to g + g \\
&\quad (q \leftrightarrow \bar{q})
\end{aligned} \tag{7}
$$

where q_a and q_b denote quarks in different flavour-states a and b. In Fig. 6f) we do not show the diagram with the quartic gluon coupling which has also been included. The corresponding matrix elements were taken from [28]. These terms were included in the cross-section calculations of Duke and Owens [7] for the lower energy $\sqrt{S_{\gamma N}} \lesssim 30\,\mathrm{GeV}$, in which their contribution is small. It was on the basis of this calculation that Aurenche et al. [8] neglected these terms. However, at HERA energies, as we will show later, they make a significant contribution at low and moderate transverse momentum, and this was anticipated in [3, 8].

Next we consider the $O(\alpha^2\alpha_s^2)$ subprocess

$$\gamma + g \to \gamma + g. \tag{8}$$

This term arises from a quark box, as shown in Fig. 7. For the calculation of the cross section we used the matrix elements of Combridge [29].

The processes given by (5–7) are called the leading-logarithmic (LL) ones, since they appear in a way that is similar to the LL approach, where the hard processes are included at the lowest order (Born) level and then convoluted with the scale violating structure/fragmentation functions.

Finally, we included the $O(\alpha_s)$ corrections to the basic Compton term. The interference between the virtual diagrams in Fig. 8a) and the Born term gives an $O(\alpha^2\alpha_s)$ contribution. The real processes

$$
\begin{aligned}
&\gamma + q \to \gamma + q + g \\
&\gamma + g \to \gamma + q + \bar{q}
\end{aligned} \tag{9}
$$

contribute to the same order. In Fig. 8b) we show the $\gamma + q$ initial-state diagrams. In this part of the calculation we used the matrix elements of Aurenche et al. [8] which adopt the universal convention that is consistent with the $\overline{\mathrm{MS}}$ scheme for the proton structure functions.

The calculation of the cross sections for processes (4–9) was performed in the γp centre-of-mass system with the rapidity defined to be positive in the direction of the photon. In Fig. 9 we show the final-state photon rapidity dependence of the minima of the proton and photon partonic momentum fractions and the fragmentation parameter. In this figure $S_{\gamma p} = 30\,000\,\mathrm{GeV}^2$ and $p_T^\gamma = 5\,\mathrm{GeV/c}$. For the proton parton momentum fraction x^p the allowed range is from x_0^p to 1. The same holds for x^γ and z. The variables x_0^γ, x_0^p and z_0 all have a maximum of one. We note here that at $y^\gamma \simeq -3.0$ the photon is probed to the smallest $x_0 \simeq 3 \times 10^{-3}$ and at $y^\gamma \simeq +3.0$ the proton is probed similarly. Note also that the fragmentation parameter is symmetrical in y^γ and at $y^\gamma = 0$ it reaches its minimum value $z_0 \simeq 5 \times 10^{-2}$. At large negative rapidities (with respect to the direction of the

initial photon) we would expect a large contribution from the soft photonic constituents to the cross sections, whilst at large positive rapidities we expect the soft partons from the proton to dominate. In these cases z_0 is rather large, ~ 0.6. At larger p_T^γ, the minimum values of x_0^γ, x_0^p and z_0 are bigger. For example, for $p_T^\gamma = 20\,\text{GeV/c}$ they are 0.06 for x_0^γ and x_0^p and 0.25 for z_0 [6].

5 Cross-section calculations

The cross-section calculations were performed in the γp centre-of-mass system for $S_{\gamma p} = 30\,000\,\text{GeV}^2$. This is not a very realistic frame in which to perform the calculation for HERA since the *ep* laboratory system is very assymetrical in the longitudinal direction. However, the purpose of this study is to quantify the sensitivity of DIC scattering to the various structure functions and in this respect it is not necessary to work in the laboratory system. As has previously been mentioned, we use the full set of MRS proton structure functions together with the PM, DO and the DG parameterizations for the photon structure functions. For the fragmentation functions we use as a standard the DO set [7], since this is the only set that offers parametrizations for both quark and gluon fragmentations. The other physics parameters involved are the QCD momentum scale, which was consistently set at $Q = p_T^\gamma$, and the QCD parameter Λ_{QCD} which depends on the structure functions being used. Note that the proton and photon structure (or fragmentation) functions require different Λ_{QCD}'s. The number of flavours was set to four and the two-loop strong coupling constant was used.

5.1 The p_T^γ distribution

We previously checked our code against the only available data, the NA14 data [13] and found satisfactory agreement [5]. However, this earlier study did not incorporate the α_s^2 leading-logarithm processes and this improves the agreement at small p_T^γ. In Fig. 10 we present the p_T^γ distribution of final state photons for the HERA energy calculated with, in our opinion, the most realistic set of proton and photon structure functions, the MRSB' and DG ones respectively. For the fragmentation functions we use DO. We calculate the p_T^γ distribution from 5 GeV/c to 80 GeV/c which is approximately the maximum p_T^γ accessible at this energy. We did not explore the $p_T^\gamma < 5\,\text{GeV/c}$ range since here we cannot trust the calculation based on the $O(\alpha_s)$ QCD corrections [6]. From the experimental point of view photons with $p_T^\gamma < 5\,\text{GeV/c}$ will be difficult to measure. Taking the integrated luminosity for the *ep* collider HERA to be $200\,\text{pb}^{-1}$/year [30] we assume that the γp integrated luminosity will be one order of magnitude less [2]. It is clear then that this process will be measurable for p_T^γ up to 45 GeV/c. In Fig. 11 the contributions of the various components of the cross section are shown relative to the Born contribution. The perturbative higher order contributions are well under control. Note that the $O(\alpha_s^2\alpha^2)$ box term contribution is added to the $O(\alpha_s)$

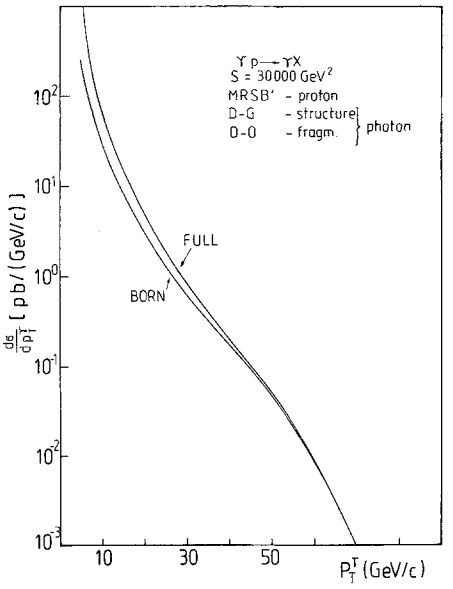

Fig. 10. The p_T^γ distribution of final-state photons produced in DIC scattering for $S_{\gamma p} = 30\,000\,\text{GeV}^2$. The lower curve is the cross section due to the Born term and the upper curve is the full cross section

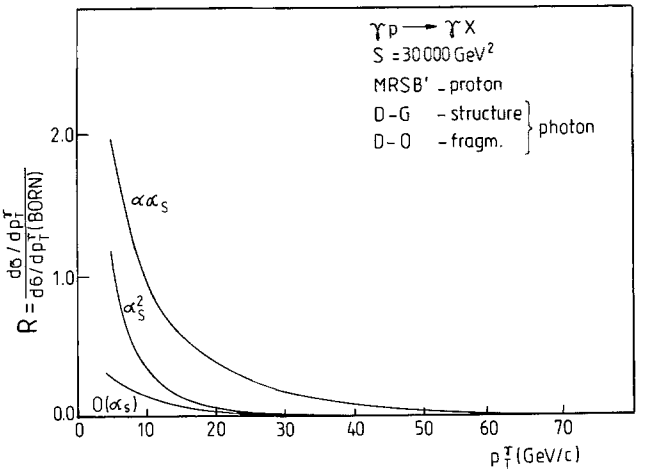

Fig. 11. Contributions of the "$\alpha\alpha_s$" and "α_s^2" leading-logarithm subprocesses and the $O(\alpha_s)$ perturbative corrections, normalized to the Born term, as a function of p_T^γ

contribution. At $p_T^\gamma = 5\,\text{GeV/c}$ this higher order correction is 28% of the Born term and at 40 GeV/c it is no more than 1%. The sum of the $\alpha\alpha_s$ leading-logarithm terms is equal to approximately two times the Born term at $p_T^\gamma = 5\,\text{GeV/c}$ and decreases to 1% at large p_T^γ. Finally, the contribution from the α_s^2 leading-logarithm terms is significant at low and moderate p_T^γ and certainly not negligible. At $p_T^\gamma = 5\,\text{GeV/c}$ it is larger than that of the Born term by approximately 20%. However, as expected it dies very rapidly with increasing p_T^γ and is negligible at 40 GeV/c.

To obtain a measure of the sensitivity to other choices of the photon structure and fragmentation functions, we calculate the p_T^γ distribution using now the PM functions

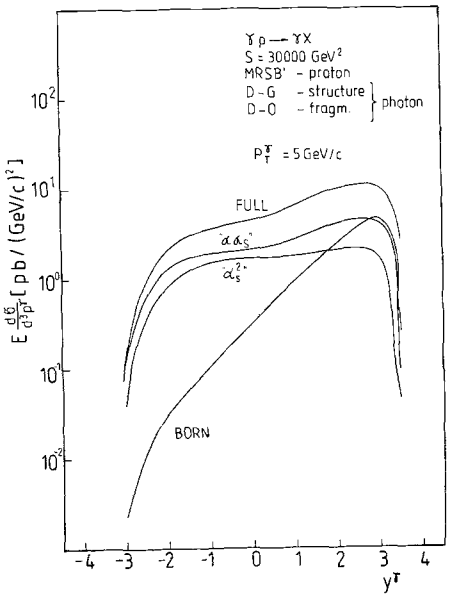

Fig. 12. The rapidity distributions of the Born, "$\alpha\alpha_s$" and the "α_s^2" leading-logarithm subprocesses at $p_T^\gamma = 5$ GeV/c. The "FULL" curve is the sum of all the processes. Note that the "$\alpha\alpha_s$" subprocesses contain either the photon structure function or the fragmentation function while the "α_s^2" subprocesses contain both. They contribute to $O(\alpha^2)$ to the DIC cross section

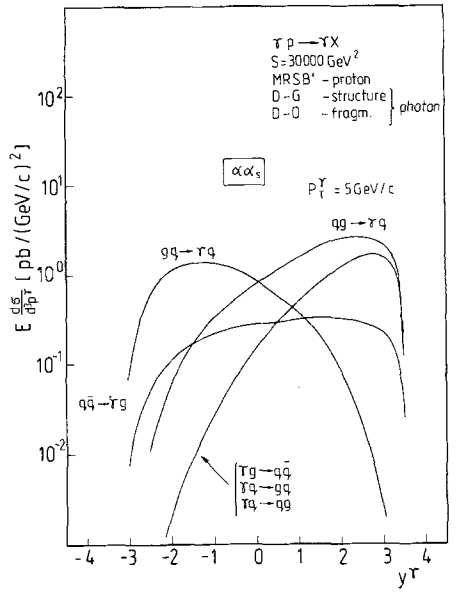

Fig. 13. The rapidity distributions of the various "$\alpha\alpha_s$" subprocesses at $p_T^\gamma = 5$ GeV/c

for the photonic quark distribution and for quark fragmentation, leaving the other inputs as before. We find that the cross section increases by 20–30% in the entire p_T^γ range. The contribution from the non-elementary photon interactions dominates for $p_T^\gamma \lesssim 17$ GeV/c, whereas with the standard set of structure and fragmentation functions described above, this occurs for $p_T^\gamma \lesssim 13$ GeV/c.

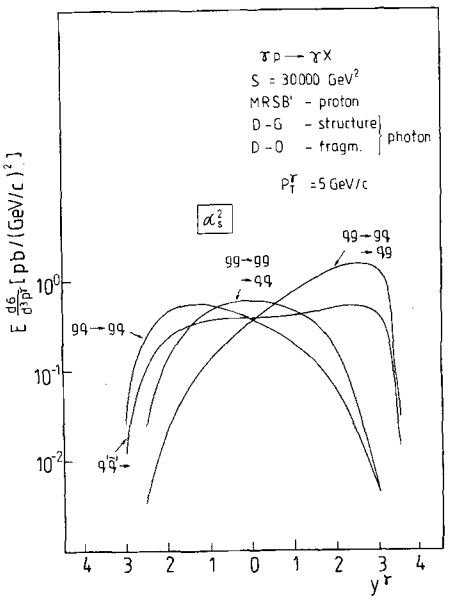

Fig. 14. The rapidity distributions of the various "α_s^2" subprocesses at $p_T^\gamma = 5$ GeV/c

5.2 *The rapidity distribution*

Previously [5] we have seen that the sensitivity of the p_T^γ distribution with respect to the proton structure functions was of the order of 10–20%. The differential cross section $E_\gamma d\sigma/d^3p_\gamma$ as a function of y^γ has the advantage of probing the full range of x-values for some particular p_T^γ and hence probe different aspects of the structure functions. In Fig. 12 we present the various contributions to this differential cross section for $p_T^\gamma = 5$ GeV/c. The structure of the Born contribution follows the earlier observation that the proton is probed to small x in the forward direction. In addition, the domination of the leading-logarithm terms at negative rapidities follows from the coming into play of the soft constituents of the photon. In Figs. 13 and 14 we separate out the various $\alpha\alpha_s$ and α_s^2 contributions. The gluon distributions in both the proton and the photon are much larger at small x than the respective quark distributions. Thus the process $g + q \to \gamma + q$ dominates in the negative rapidity region while the $q + g \to \gamma + q$ term peaks in the positive rapidity region (see Fig. 13). The gg scattering terms in Fig. 14 are approximately symmetrical with respect to the rapidity and this is an indication that the gluons in the photon and proton are not very different. Below we estimate the rate for the production of photons with $p_T^\gamma = 5 \pm 0.5$ GeV/c and at interesting rapidities within an interval $\Delta y^\gamma = 1$.

We must emphasise that in the negative rapidity region the differential cross section is dominated, to $O(80\%)$, by subprocesses which originate from the gluonic content of the photon. The sum of these contributions peaks at $y^\gamma \simeq -1.5$ rather than at $y^\gamma \simeq -2.9$ (as one might

expect from Fig. 9), due to the interplay between the proton and photon structure functions, and this will facilitate the measurement of this cross section in the laboratory frame – as we shall discuss later.

Using the DG photon structure function and the DO fragmentation functions we varied the proton structure function to determine the sensitivity of the rapidity distributions to the various parametrizations. In Fig. 15 we present the cross sections due to the various MRS sets. MRS1, which is not shown in the figure (see [6]), and MRSE′ produce almost identical cross sections at negative rapidities while MRS1 and MRSB′ produce similar cross sections at positive rapidities. The difference between the MRSE′ and MRSB′ cross sections at small x (or at positive rapidity ~ 2–3) is about 20%. At very small x the $1/\sqrt{x}$ gluon in MRS3 dominates. The sensitivity of the process to the EMC-BCDMS quark distribution differences is at best 25%. In the large positive rapidity region, using the standard set of parton parametrizations, we could expect, for the quoted luminosity above, some 6000 events per annum in the p_T^γ and rapidity domain described above and the 20% difference in the cross sections may be discernable. However, this sensitivity may be blurred somewhat by the fact that the MRSB′ set has a $\Lambda_{\overline{\text{QCD}}} = 200\,\text{MeV}$ as compared to $\Lambda_{\overline{\text{QCD}}} = 100\,\text{MeV}$ for the MRSE′ set. This will affect the value of α_s in a way which enhances the cross section of the MRSB′ set.

The sensitivity of the rapidity distribution to the different photon structure function parametrizations is investigated in Fig. 16, where the proton structure function is held fixed (MRSB′). At $y^\gamma \sim +3.0$ and $y^\gamma \sim -2.0$ the invariant cross sections have maxima for the DO and PM cases and at these rapidities the PM cross section is two times as large as the DG one. At large positive rapidities, that is at large x^γ the cross sections due to the DG and the DO parametrizations coincide. This is expected since the quark distributions in the two sets are very similar at large x^γ. For $y^\gamma \sim -2.5$ the DO cross section is about 1.7 times the magnitude of the DG one. The PM approach predicts about 12500 events per year in an interval $\Delta y^\gamma = 1$ around the maximum cross section at positive rapidity and about 3000 events in the same interval around the corresponding maximum at negative rapidity. Note that for the fragmentation function we used the DO parametrization in all these cases.

Finally we investigated the sensitivity of the DIC process to the gluon and quark fragmentation functions by fixing the proton and photon structure functions and changing the fragmentation function for the gluon from that of DO to that of DG and for the quark from that of DO to that of the PM prediction. In the former case, as mentioned earlier, we let $D_{\gamma/g} = F_{g/\gamma}$ in the DG case. First we compared the cross sections due to the DO and DG gluon fragmentation functions of the sum of the entire set of subprocesses which involve the fragmentation of a final-state gluon into a photon. These are represented by the solid lines in Fig. 17. These curves differ by up to a factor of 3.3 where the cross section is sizeable. Next we consider the sum of those processes that have a final-state quark fragmenting into a photon. The cross

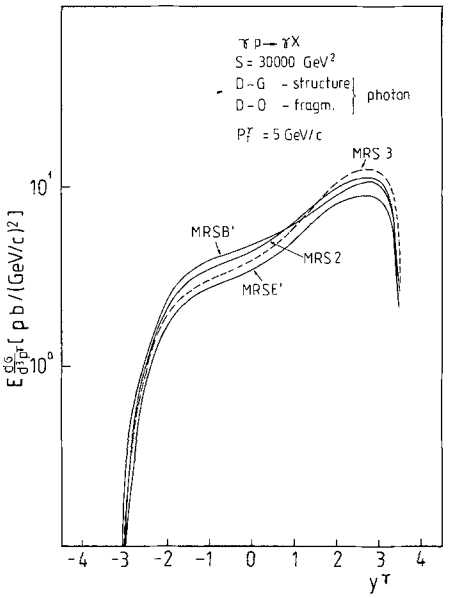

Fig. 15. The dependence of the full invariant cross section on the various proton structure functions is shown as a function of rapidity. The photon structure function (DG) and the fragmentation functions (DO) are fixed. The transverse momentum of the final state photons is $p_T^\gamma = 5\,\text{GeV/c}$

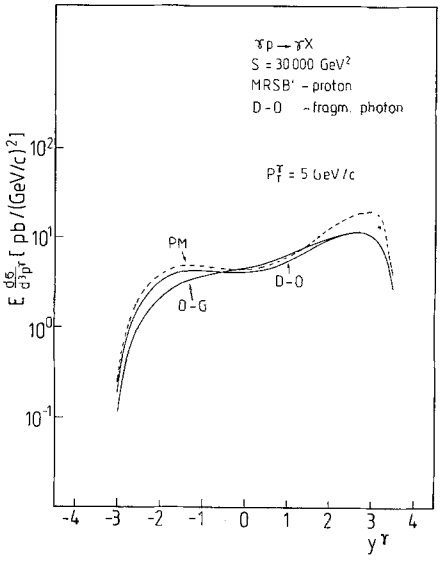

Fig. 16. The dependence of the full invariant cross section on the various photon structure functions plotted as a function of rapidity. The proton structure function (MRSB′) and the fragmentation functions (DO) are fixed. The transverse momentum of the final state photons is $p_T^\gamma = 5\,\text{GeV/c}$

sections due to the DO quark fragmentation function and the PM one, which are the only ones available, are represented by the dashed lines in Fig. 17. These cross sections are substantial and are certainly measurable. As we shall show in the topological studies of the final-states described below, the fragmentation terms are distinguishable from the rest of the cross section. In a $\Delta y^\gamma = 1$ interval around $y^\gamma = 2.5$ the PM predicts that the number of

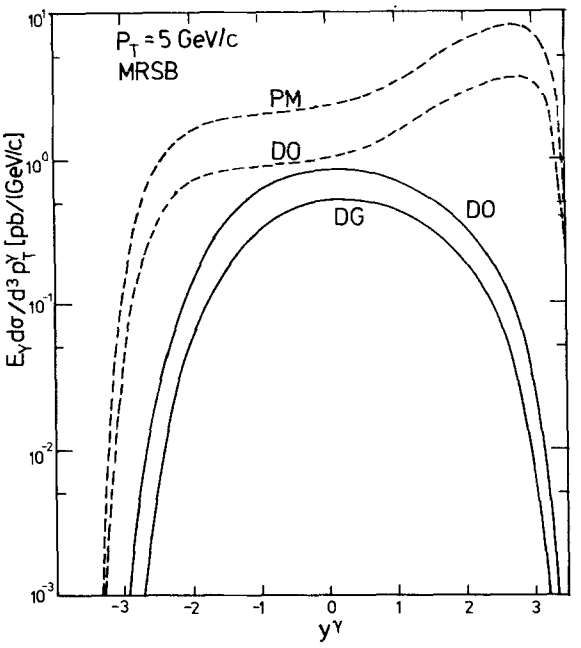

Fig. 17. The dependence of the rapidity distribution of final-state photons at $p_T^\gamma = 5\,\text{GeV/c}$ on the various fragmentation functions. The solid lines show the cross sections of the sum of all the subprocesses in which a final-state gluon fragments for each of the two parametrizations. The dashed curves are the distributions due to the sum of the subprocesses in which a final-state quark fragments into a photon. Here we used the parton model quark fragmentation function and the DO one

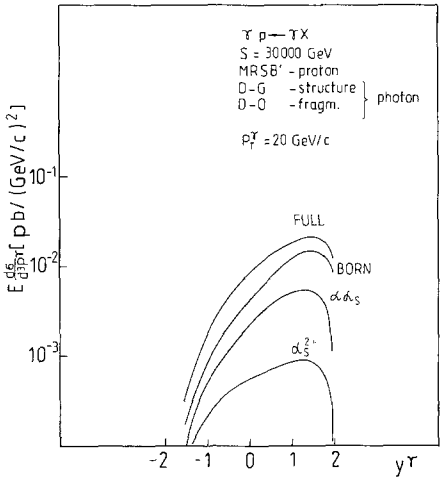

Fig. 18. The rapidity distribution of final state photons produced in DIC scattering at a transverse momentum of $p_T^\gamma = 20\,\text{GeV/c}$. The Born, "$\alpha\alpha_s$", "$\alpha_s^2$" contributions are shown together with the full cross section. The $O(\alpha_s)$ perturbative corrections are too small to be shown on this scale

events per annum will be of $O(5000)$ and this should allow a detailed study of this particular function. the 'background' from gluon fragmentation in this rapidity region is of the order of 100 events in the DO approach.

Finally we perform a rapidity distribution calculation for $p_T^\gamma = 20\,\text{GeV/c}$. In Fig. 18 we show the various contributions, and as expected that of the leading-

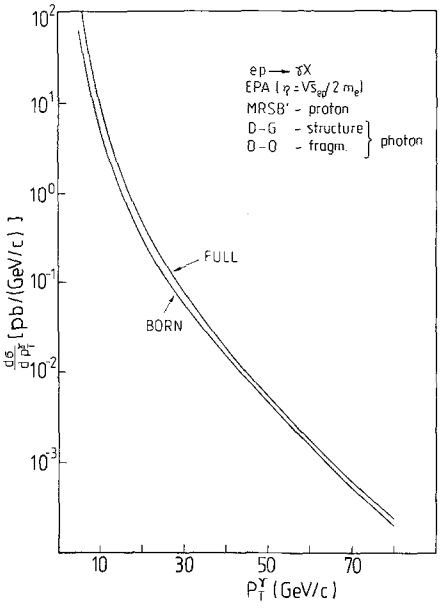

Fig. 19. The transverse momentum distribution of final-state photons in the process $e + p \to \gamma + X$, where the initial state photons are produced assuming the equivalent photon approximation. The curve marked 'FULL' is the cross section with contributions from the full set of subprocesses

logarithm terms is significantly smaller than the Born one. In addition the event rate at any particular rapidity will not exceed 2–3 events per annum and this will not permit any structure function discrimination.

5.3 The ep laboratory frame

In order to estimate the rate for the deep inelastic Compton process in *ep* collisions at HERA we perform the calculation of the p_T^γ distribution by generating an energy spectrum of initial-state photons based on the equivalent photon approximation (EPA). We have assumed the usual leading-order form of this approximation [31]

$$G(x) = \frac{\alpha}{2\pi} \log \eta \frac{[1+(1-x)^2]}{x}, \tag{10}$$

where $\eta^2 = S_{\gamma p}/4m_e^2$. The results are presented in Fig. 19. One can expect about 272 pb for $p_T^\gamma > 5\,\text{GeV/c}$, 31 pb for $p_T^\gamma > 10\,\text{GeV/c}$ and 3 pb above 20 GeV/c.

From simple kinematical considerations it is clear that the configurations of the final-states which correspond to various subprocesses are distinct from each other – this will allow the isolation of these subprocess contributions. The asymmetric *ep* kinematics at HERA will be very helpful here. We discuss only the $p_T^\gamma = 5\,\text{GeV/c}$ case, since it is here that we expect the largest effects due to the leading-logarithmic subprocesses. A more detailed study demands a Monte Carlo approach, and this work is now in progress [22]. From Fig. 9 we see that the smallest x's in the case of the proton and the photon are reached at rapidities of ~ 2.9 and

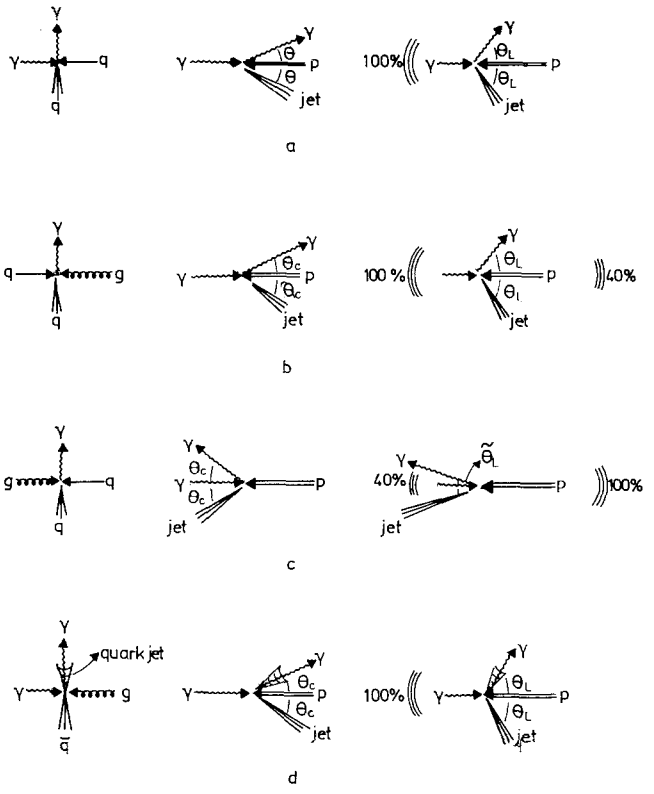

Fig. 20 a–d. The topology of the most important subprocess in each category of final state studied in the parton centre-of-mass system, the γp centre-of-mass system and in the laboratory system; **a** the Born term: $\gamma + q \to \gamma + q$, **b** gluon in proton: $q + g \to \gamma + q$, **c** gluon in photon: $g + q \to \gamma + q$, **d** fragmentation: $\gamma + g \to q + \bar{q}$. The angles are $\theta_c \simeq 6°$, $\theta_L \simeq 55°$ and $\theta_L \simeq 1°$. The spectator jets from the proton are denoted by (((and))), respectively. The percentages indicate the fraction of the incident particle energy carried by the relevant spectator jets

~ -2.9 in the γp centre of mass system, respectively. This corresponds to 90° scattering at the parton level. From the rapidity plot presented above it is clear that as a first approximation these regions of rapidities are responsible for the dominant contributions to the cross section. Taking this into account we present in Fig. 20 the characteristics of the final state of the most important subprocesses: a) the Born term, b) $qg \to \gamma q$, c) $gq \to \gamma q$, and d) $\gamma g \to q\bar{q}$ where the final quark fragments into a photon. We present here the situation as seen in the parton centre-of-mass system (CM), in the γp centre-of-mass frame (CM) and in the ep laboratory system (LAB). It seems to be possible to distinguish these processes, one from the other, even if they contribute to the final-states in the same phase space region as in example a) and b) above. For instance, the observation of the presence or the absence of the spectator jets from the photon or the proton may help to isolate the one from the other (see Fig. 10). Note that in cases a), b) and d) the fragments of the incident proton carry almost all of its energy (denoted by 100% in the Fig. 20) whereas in case c) the fragments carry only 40% of the proton energy. For the incident photon the situation in cases b) and c) is opposite while in a) and d) a spectator jet from the photon is not expected. To observe the events resulting from the fragmentation process it would be important to be able to detect photons accompanied by a jet as in case d). Note that in these events we have hard fragmentation since $z_0 > 0.6$ (see Fig. 9). The most interesting case would be to see hard photons in the backward direction, since they would carry information about the gluon content of the photon (case c). The subprocesses involving nonelementary initial *and* final state photons will also present a rather clear signature.

In order to probe the gluon structure of the photon it will be crucial to measure the DIC cross section at relatively small transverse momenta, say $p_T^\gamma = 5\,\text{GeV/c}$, and large negative rapidities in the γp centre-of-mass system. This corresponds to very small angles $\tilde{\theta}_L$, with respect to the proton direction, in the ep laboratory system. The configurations that were considered above were based on the assumption that the dominant scattering occurs at 90° in the partonic centre-of-mass system (CM) and this corresponds to a rapidity $y_{CM}^\gamma = -2.9$. However, a study of Figs. 12 and 14 indicates that in practice the peak due to the scattering of the gluons from the photon is shifted to $y_{CM}^\gamma = -1.5$ corresponding to a laboratory angle $\tilde{\theta}_L \simeq 3°$ which is more accessible experimentally.

The gluonic component of the proton produces a large contribution to the DIC scattering at $p_T^\gamma = 5\,\text{GeV/c}$ and at large positive rapidities, that is $y_{CM}^\gamma \simeq 2.5$, as can be seen in Figs. 12 and 14. Therefore the assumption of the underlying parton configurations discussed qualitatively above is better justified in this case. This rapidity corresponds in the ep laboratory frame to an angle $\theta_L \sim 76°$, with respect to the direction of initial-state photon. Note that in Fig. 20 the angle $\theta_L = 55°$ corresponds to a rapidity of 2.9.

The Born and box subprocesses contribute significantly in a similar domain of phase space, as do the subprocesses with a gluon from the proton. These contributions which are only slightly separated in the centre-of-mass system are widely separated in the ep laboratory frame due to the large boost. The Born contribution peaks at the ep laboratory angle of $\simeq 55°$ while the box contribution peaks at $\simeq 40°$ with respect to the photon direction. It would appear then that HERA offers, for the first time, the opportunity to measure the box diagram contribution. Past estimates [8] indicated that this appeared difficult. However, further study is required to consider the effect of the smearing of the initial-state photon energies [22].

6 Conclusions

DIC scattering will be measurable at HERA up to $p_T^\gamma \simeq 45\,\text{GeV/c}$. For most of this study we have used a fixed energy photon beam ($\sim 9\,\text{GeV}$) which is clearly a simplification. The convolution of the cross section with the equivalent photon approximation produces a more realistic picture, as has been discussed above.

The event rates are sufficiently high for the process to be studied in its own right as a test of perturbative QCD. The complete next-to-leading order corrections to the cross section are small and well under control.

However, the leading-logarithmic contributions which arise from the non-elementary behaviour of the photon dominate the differential cross section for $p_T^\gamma \lesssim 15\,\mathrm{GeV/c}$ and the region $5\,\mathrm{GeV/c} \lesssim p_T^\gamma \lesssim 15\,\mathrm{GeV/c}$ offers the opportunity to study the quark and gluon distributions in the photon and proton.

To investigate this possibility we studied in detail the invariant cross section $E_\gamma d\sigma/d^3p_\gamma$. The gluonic content in the proton is probed to small x at large positive rapidities and while the sensitivity of the process to the various MRS structure functions does not exceed 20–25%, DIC scattering will present the opportunity to study the quark distributions in the proton in an (x, Q^2) region which will complement DIS. Importantly, DIC scattering at HERA offers an opportunity to make a clean study of the gluon distributions in the photon. We estimate again that in a $\Delta y^\gamma = 1$ interval about $y^\gamma \sim -1.5$ and using the usual set of parametrizations, HERA will produce $O(2500)$ events per annum on which to base this study. In addition, the process is sensitive to the different gluon distribution – the DO structure function producing a cross section that is twice as large as the DG one at $y^\gamma = -1.5$, where this component of the cross section dominates.

DIC at HERA will allow the study of the quark-to-photon fragmentation function. The event rates are large and the configuration of the final-state, that is a photon inside a quark jet, will make this measurement possible. The study of the gluon fragmentation function will be extremely difficult since the contribution of the subprocesses with a final-state gluon fragmenting is always dominated by the contribution of the subprocesses with a fragmenting final-state quark by two orders of magnitude.

HERA's asymmetric kinematics facilitate these structure function studies. The large boost from the centre-of-mass system to the *ep* laboratory system affects the topologies of the different final-states. For instance, the final-states of the subprocesses that arise from the gluon content of the proton peak at a rapidity of $y^\gamma \simeq 2.5$, which corresponds to a small centre-of-mass angle, measured with respect to the photon direction. However, in the *ep* laboratory system this peak will be observed at an angle of $\sim 76°$. While this adversely affects the contribution due to the gluonic content of the photon where $\tilde{\theta}_L = 3°$ with respect to the proton momentum, we indicated earlier that it should still be measurable at HERA.

The Born and box cross sections for $p_T^\gamma = 5\,\mathrm{GeV/c}$ peak in a very similar phase space region in the centre-of-mass system. However, the boost separates them in the *ep* laboratory system and they may be observable separately. In addition, these contributions to the total cross sections are topologically unique and if they are separated in angular terms the box diagram contribution will be measurable.

We conclude that DIC scattering at HERA provides the opportunity to measure the structure of the photon and the quark-to-photon fragmentation function. However, further studies are necessary to take into account the experimental conditions at HERA; such as the spread in the initial-state photon energy, the possible backgrounds (in particular that due to final-state π^0's) and experimental cuts. A Monte Carlo study in under way [22].

Finally, we should mention that other processes can provide complementary information on the photon structure functions. Examples are J/ψ production, lepton pair production, and large p_T jet production. Although the cross sections for these are significantly larger than the DIC cross sections at the same p_T, the latter have the advantage that the photon is a more direct probe with a more precisely measurable momentum. In addition, DIC scattering provides us with a unique opportunity to study the quark fragmentation function and possibly the box diagram.

Acknowledgements. We are grateful to M. Drees, R. Godbole and A. Levy for helpful discussions and for reading the manuscript. We would also like to thank W. Buchmüller and G. Wolf for interesting discussions. One of us (MK) would like to thank P. Chiapetta and P. Mery of the Centre de Physique Theorique, Marseilles where part of this work was completed, for their very warm hospitality. ACB is grateful to the Foundation for Research Development for an ad-hoc grant. ACB and MK would like to thank the Theory Group at DESY for their warm hospitality and ACB is grateful for financial support.

References

1. J. Feltesse: Proceedings of HERA Workshop, R.D. Peccei (ed.), Hamburg, October 1987
2. B. Diekmann, F.D. Gebert, R. Seifert: Proceedings of HERA Workshop, R.D. Peccei (ed.), Hamburg, October 1987
3. P. Aurenche et al.: Proceedings of HERA Workshop, R.D. Peccei (ed.), Hamburg, October 1987
4. J.J. Engelen: Proceedings of the Workshop on experimentation at HERA, Nikhef, Amsterdam, DESY HERA 83/20
5. A.C. Bawa, W.J. Stirling: J. Phys. G14 (1988) 1553
6. M.A. Krawczyk; IFT 7/89, to appear in Acta Phys. Pol. B21 (1990)
7. D.W. Duke, J.F. Owens: Phys. Rev. D26 (1982) 1600; Erratum: Phys. Rev. D28 (1983) 1227
8. P. Aurenche et al.: Z. Phys. C – Particles and Fields 24 (1984) 309
9. M. Krawczyk, unpublished
10. A. Czechowski, M. Krawczyk: Nucleonika 26 (1981) 1175; A.D. Contogouris et al.: Phys. Rev. D25 (1982) 1280
11. A. Czechowski et al.: Z. Phys. C – Particles and Fields 19 (1983) 35
12. J.D. Bjorken, E.A. Paschos: Phys. Rev. 185 (1969) 1975
13. P. Astbury et al. (NA14 Collaboration): Phys. Lett. 152B (1985) 149
14. E. Witten: Nucl. Phys. B120 (1977) 189
15. D.W. Duke, J.F. Owens: Phys. Rev. D22 (1980) 2280
16. Ch. Berger, W. Wagner: Phys. Rep. 146 (1987) 1
17. J. Kuti, V.F. Weisskopf: Phys. Rev. D4 (1971) 3418
18. P. Aurenche, et al.: Phys. Rev. D39 (1989) 3275
19. G. Altarelli, G. Parisi: Nucl. Phys. B126 (1977) 298
20. R.S. Fletcher, et al.: Phys. Lett. B225 (1989) 176
21. M. Drees, R. Godbole: Phys. Rev. Lett. 61 (1988) 682 and Phys. Rev. D39 (1989) 169
22. A.C. Bawa, M.A. Krawczyk: in preparation
23. M. Drees, F. Halzen: Phys. Rev. Lett. 61 (1988) 61; More recently: T.K. Gaisser, et al.: MAD/PH/557 (1990)
24. M. Drees, D. Grassie: Z. Phys. C – Particles and Fields 28 (1985) 451

25. A.D. Martin, R.G. Roberts, W.J. Stirling: Phys. Rev. D37 (1988) 1161
26. A.D. Martin, R.G. Roberts, W.J. Stirling: Phys. Lett. 206B (1988) 327
27. A.V. Efremov, S.V. Ivanov: Dubna preprint E2-83-367 (1983)
28. J.F. Owens, et al.: Phys. Rev. D18 (1978) 1501
29. B.L. Combridge: Nucl. Phys. B174 (1980) 243
30. G. Ingelman, R. Ruckl: Proceedings of HERA Workshop, R.D. Peccei (ed.), Hamburg, October 1987
31. Min-Shih Chen, P. Zerwas: Phys. Rev. D12 (1975) 1987